Front. Phys. 13(2), 134204 (2018)
https://doi.org/10.1007/s11467-017-0740-4

RESEARCH ARTICLE

Spontaneous ferroelectricity in strained low-temperature monoclinic Fe_3O_4: A first-principles study

Xiang Liu, Wen-Bo Mi†

Tianjin Key Laboratory of Low Dimensional Materials Physics and Processing Technology, School of Science, Tianjin University, Tianjin 300354, China
Corresponding author. E-mail: †miwenbo@tju.edu.cn
Received October 21, 2017; accepted November 24, 2017

As a single-phase multiferroic material, Fe_3O_4 exhibits spontaneous ferroelectric polarization below 38 K. However, the nature of the ferroelectricity in Fe_3O_4 and effect of external disturbances such as strain on it remains ambiguous. Here, the spontaneous ferroelectric polarization of low-temperature monoclinic Fe_3O_4 was investigated by first-principles calculations. The pseudo-centrosymmetric FeB42–FeB43 pair has a different valence state. The noncentrosymmetric charge distribution results in ferroelectric polarization. The initial ferroelectric polarization direction is in the $-x$ and $-z$ directions. The ferroelectricity along the y axis is limited owing to the symmetry of the Cc space group. Both the ionic displacement and charge separation at the FeB42–FeB43 pair are affected by strain, which further influences the spontaneous ferroelectric polarization of monoclinic Fe_3O_4. The ferroelectric polarization along the z axis exhibits an increase of 45.3% as the strain changes from 6% to −6%.

Keywords spontaneous ferroelectric polarization, charge ordering, biaxial strain, Berry phase, modern theory of polarization

PACS numbers 42.25.Ja, 75.50.Gg, 77.80.B-, 77.80.bn

1 Introduction

Recently, multiferroic materials that combine ferroelectricity, ferromagnetism, and ferroelastic characteristics have made it feasible to realize complex functional devices and have attracted much interest because of the ability of changing their magnetic states through application of electric fields and vice versa [1–3]. The ferroelectric (FE) polarization switch in a multiferroic tunnel junction can realize multiple-resistance states, which can enhance the storage density [4–8]. Low energy consumption and high response in multiferroic heterostructures provide potential applications in next-generation sensors and spintronics devices [9–12]. As a natural magnet, Fe_3O_4 has been used for thousands of years. Nowadays, Fe_3O_4 has attracted considerable attention and is considered to be a candidate for spintronics devices owing to its high Curie temperature of 858 K [13], theoretical spin polarization of −100% [14], and large net magnetic moment of $\sim 4\mu_B$/f.u. [15]. A first-order phase transition, which is known as the Verwey transition, has been observed in the temperature-dependent conductivity of Fe_3O_4 at $\sim$ 120 K (T_V) [16], where the conductivity changes by about two orders of magnitude across T_V. Below T_V, the unit cell distorts to a $\sqrt{2}a \times \sqrt{2}a \times 2a$ monoclinic superstructure with a Cc space group, where a is the lattice constant of cubic Fe_3O_4. Fe_3O_4 exhibits FE behavior below 38 K [17] and magnetoelectric coupling at 4.2 K [18]. Yamauchi *et al.* [19] have studied the spontaneous FE polarization in Fe_3O_4 by using first-principles calculations. The FE polarization along the x, y, and z axes are about −4.41, 0, and 4.12 μC/cm^2, respectively [19]. However, several experimental results indicate a significant difference. At 4.2 K, Kato *et al.* [20] reported an FE polarization of 1.5 μC/cm^2 along $[001]_m$, while a large FE polarization of 52 μC/cm^2 along $[100]_m$ was reported by Miyamoto *et al.* [21]. Recently, Alexe *et al.* [17] investigated the ferroelectricity of Fe_3O_4 in metal/Fe_3O_4/Nb-doped $SrTiO_3$ heterostructures, which were prepared by pulsed laser deposition (PLD) and magnetron sputtering (MS). At $\sim$ 10 K, the switchable FE polarization (2**P**) projected onto the x–y plane is $\sim$ 11 (PLD) and $\sim$ 5 μC/cm^2 (MS). There are two possible explanations

*arXiv: 1712.02524.

for the different experimental results. First, leakage, antiphase boundaries, or residual strain may hamper the FE polarization measurements [20]. Second, the discrepancy can be illustrated by the modern theory of polarization, which recognizes FE polarization as a superposition of lattices rather than of vectors [22–25]. In this paper, a series of investigations on the origin and direction of spontaneous FE polarization and strain effects on ferroelectricity in low-temperature monoclinic Fe_3O_4 are performed. Remarkably, the FE polarization shows an increase of 45.3% as the strain changes from 6% to −6%, which has potential applications in multiferroic devices.

2 Calculation details and models

Electronic structure calculations were performed based on density functional theory and the generalized gradient approximation using the Vienna Ab-initio Simulation Package (VASP) [26, 27]. The projector-augmented-waves method was used to describe the core electrons. The Perdew–Burke–Ernzerhof exchange-correlation functional parameterization within the generalized gradient approximation (GGA) was used. The energy cutoff and the Monkhorst–Pack grid of k points were set as 400 eV and $3\times3\times2$, respectively. The on-site Column interaction parameter $U = 4.5$ eV and the on-site exchange interaction parameter $J = 0.89$ eV for Fe ions were used [28–31]. The lattice constants, atomic labels, and positions of low-temperature monoclinic Fe_3O_4 were selected from Ref. [32], where $a = 11.88881$ Å, $b = 11.84940$ Å, $c = 16.77515$ Å, and $\beta = 90.2363°$. The structure optimizations were stopped when the total energy change became $< 10^{-5}$ eV and the Hellman–Feynman force change of the optimized structure fell below 10^{-2} eV/Å. After structural optimization, the unit cell showed a bit of expansion, where $a = 11.88549$ Å, $b = 11.88974$ Å, $c = 16.78531$ Å, and $\beta = 90.1760°$.

Lattice strain ranging from 6% to −6% is defined as $S = (b - a)/a \times 100\%$, where S, a, and b are the strain and the lattice constants without and with strain, respectively. Both tensile and compressive strains were imposed along the x and y axes. The calculations applied with lattice strain were based on the optimized structure, where the in-plane lattice constant was calculated through the upper equation and fixed through the optimization. The out-of-plane lattice constant was selected from the former optimized result and relaxed through the optimization. The Berry phase was calculated to determine the contribution of FE polarization from both ions and electrons. To distinguish the spontaneous FE polarization, a paraelectric (PE) structure must be considered because the value of polarization for a PE structure is not always zero [25]. Here, a centrosymmetric Fe_3O_4 with $C2/c$ symmetry as a conference structure was built to simulate the zero-polarization state in a coercive electric field. The PE structure with $C2/c$ symmetry, which is a subgroup of Cc symmetry, was obtained by an online server [33–35]. Several intermediate structures were constructed between FE and PE structures. Although the exact displacements through FE polarization switching were more complicated, all of the ions were assumed to move through a linear path. The displacement of ions was scaled by λ, where $\lambda = 100\%$ and $\lambda = 0\%$ represent Cc (FE) and $C2/c$ (PE) structures, respectively. When the sample was further polarized to a negative polarization state, the ions moved to a symmetric position according to the reference structure in the experiment. Thus, negative λ, i.e., the enantiomorphic counterpart with $-(Cc)$ structure, was also considered to simulate the sample with a negative polarization state. The FE polarization was calculated with the Berry phase, point charge model (PCM), and polarization quantum. The calculations based on the PCM were performed by using our homemade codes. The PCM calculations were based on $\boldsymbol{P} = \sum_i q_i \boldsymbol{r}_i/\Omega$, where $q_i\boldsymbol{r}_i$ represents the electric moment of the i^{th} ion with q_i charges at $\boldsymbol{r}_i$, Ω is the volume of the unit cell, and $\boldsymbol{r}_i$ is treated as a vector from the body center to the i^{th} ion within our codes. Ions at vertices, face centers, and edges were placed at all of the equivalent sites to eliminate extra FE polarization throughout the PCM calculations.

3 Results and discussion

Figure 1(a) shows the lattice structure of low-temperature monoclinic Fe_3O_4. It is found that Fe_3O_4 with the Cc space group has a pseudo-centrosymmetric structure. Thus, the artificial centrosymmetric Fe_3O_4 with the $C2/c$ space group has a similar structure (not shown here). First, the electronic structure in both FE and PE phases was compared. All of the pseudo-centrosymmetric ion pairs in the FE phase, except for the FeB42–FeB43 pair [in Fig. 1(a)], possess a similar density of states (DOS), which suggests a similar valence state for the counterpart. Figures 1(b)–(d) show the partial DOS projected onto 3d orbits of FeB42 and FeB43 at $S = 0\%$ and $\lambda = 100\%$. It is noted that the ionic sites at FeB42 and FeB43 are equivalent within $C2/c$ symmetry. In Fig. 1(b), the DOS at FeB42 (FeB43) does not exhibit a band gap, but the occupation state at the Fermi level is zero. The valence of FeB42 (FeB43) with $C2/c$ symmetry is more like +2.5. In the FE phase, the spin-down t_{2g} band is occupied at FeB42 [Fig. 1(c)] and unoccupied at FeB43 [Fig. 1(d)] at $\lambda > 0\%$, where the valence states of FeB42 and FeB43 are divalent-like and trivalent-like, respectively. At $\lambda < 0\%$, the occupa-

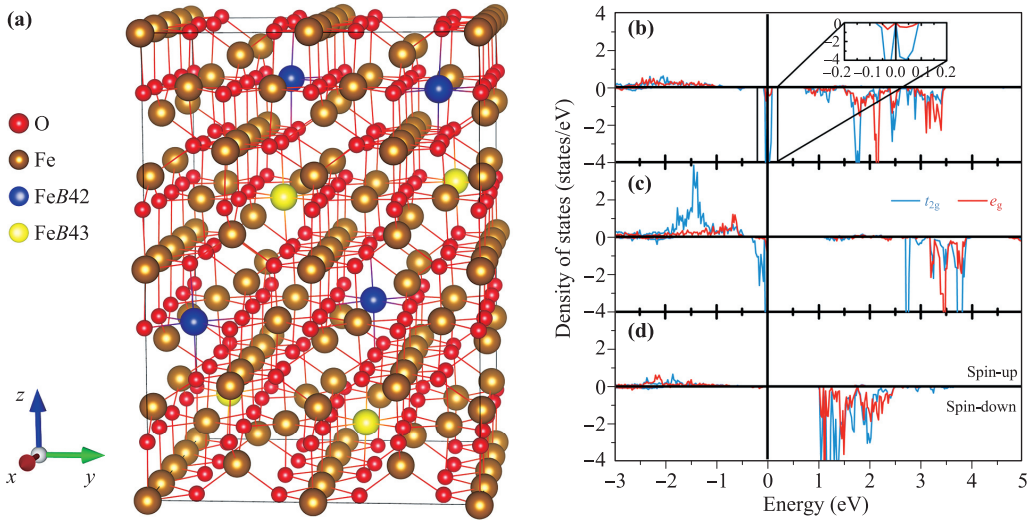

Fig. 1 **(a)** Lattice structure of low-temperature monoclinic Fe_3O_4 with the Cc space group. FeB42 and FeB43 are colored with blue and yellow, respectively. **(b)** DOS of FeB42 (FeB43) with $C2/c$ symmetry. The inset shows the magnification of DOS at -0.2 eV $\leq E \leq 0.2$ eV. **(c, d)** DOS of FeB42 and FeB43 within Cc symmetry.

tion states are inverted, which manifests inversed valence states. Thus, we suppose that the FE polarization comes from the noncentrosymmetric charge distribution at the FeB42–FeB43 pair.

It should be pointed out that the Berry phase results cannot confirm the direction of FE polarization and distinguish the polarization from that of a single ion. In this point of view, the PCM was used to calculate the FE polarization. Here, the results based on the PCM provide only a rough estimate. Figure 2 shows the dependence of FE polarization on ionic displacement and charge separation at $S = 0\%$. The charge separation is defined by the difference of valence between trivalent-like and divalent-like ions. The FE polarization along the y axis is forbidden owing to the symmetry limitation. The FE polarization increases as charge separation is enhanced but decreases with increased ionic displacement. One can see that the low-temperature monoclinic Fe_3O_4 has FE polarization when the lattice structure loses centrosymmetry. In Fig. 2, the shining balls in each color map represent the FE polarization from the FeB42–FeB43 pair. It is hard to distinguish the color of shining balls from the background, which demonstrates that the FE polarization in monoclinic Fe_3O_4 almost comes from the FeB42–FeB43 pair. Similar results were also found with other strains (not shown here). We can conclude that once Fe_3O_4 loses its centrosymmetry, the equivalent Fe$B42^{2.5+}$–Fe$B43^{2.5+}$ pair will divide into divalent-like and trivalent-like ions. The noncentrosymmetric charge distribution of the FeB42–FeB43 pair results in FE polarization in monoclinic Fe_3O_4. The absence of FE polarization at temperatures just below T_V can be ascribed to the low resistance of Fe_3O_4, which results in a large current leakage [17]. PCM calculations yield the

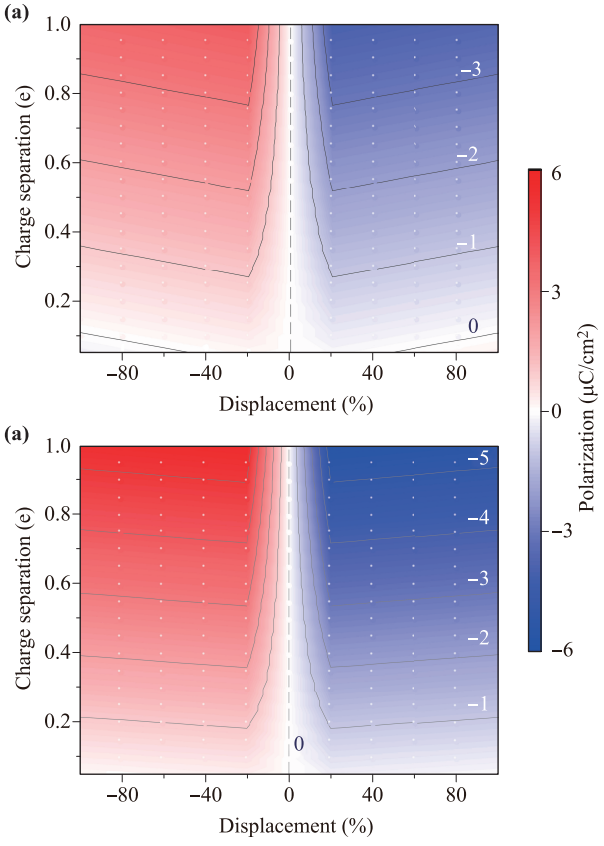

Fig. 2 Ferroelectric polarization along **(a)** the x axis and **(b)** the z axis calculated with the PCM at $S = 0\%$. The color scale is shown in the right column. Gray lines indicate isolines of the FE polarization.

direction of FE polarization. The FE polarization from other ions can be treated as zero. The FE polarization

direction of the FeB42–FeB43 pair is the direction of FE polarization for monoclinic Fe_3O_4. A vector $\boldsymbol{R}$ from the body center to the center of the FeB42–FeB43 pair was defined as $\boldsymbol{r}_{FeB42} + \boldsymbol{r}_{FeB43}$ and calculated. At $S = 0\%$ and $\lambda = 100\%$, $\boldsymbol{R} = (0.128, 0, 0.116)$ Å, which indicates that the center of the FeB42–FeB43 pair is away from the body center along $+x$ and $+z$ directions. However, FE polarization was along the $-x$ and $-z$ directions owing to a higher valence of FeB43. The initial FE polarization direction was different from the $-x$ and $+z$ directions as reported by Yamauchi *et al.* [17].

Figure 3 shows the dependence of FE polarization obtained by Berry phase calculations and total energy on the ionic displacement at $S = 0\%$, $\pm2\%$, $\pm4\%$, and $\pm6\%$. In Fig. 3(a), the FE polarization of enantiomorphic counterpart structures exhibits similar values but an inverse direction. The positive (negative) value represents that the direction of FE polarization was in the plus (minus) direction of coordinates. The opposite value of FE polarization in enantiomorphic structures comes from the inverse valence state of FeB42–FeB43 in the relevant structures. In Fig. 3(b), Fe_3O_4 with enantiomorphic structures possesses a similar total energy, which stabilizes at $\lambda = \pm100\%$ except for $S = 2\%$. The artificial $C2/c$ structure is unstable based on the calculations. Unlike the results of ferroelectricity in $BiFeO_3$ [25], FE polarization of Fe_3O_4 does not show a linear-like dependence on displacement. As we know, polarization in a limited three-dimensional system is defined as $\boldsymbol{P} = \sum_i q_i \boldsymbol{r}_i / \Omega$, where the FE polarization shows a linear correlation with the ionic distribution. However, the calculated results seem unreasonable at first sight. In common perovskite (ABO_3) ferroelectrics, FE polarization arises from the B-ion displacement [25, 36, 37], whereas, in Fe_3O_4, FE polarization is dominated by charge separation at the FeB42–FeB43 pair, namely, the nature of charge ordering in Fe_3O_4 below T_V rather than ionic displacement.

To investigate the strain effects on charge separation at the FeB42–FeB43 pair, the bond-valence sum (BVS) [38–40] was calculated to estimate the ionic valence. The bond-valence sum of the ion, BVS $= \sum_i^n \exp[(R_0 - R_i)/b]$, is decided by the surrounding bond lengths, where R_0 and R_i represent the bond-valence parameter and the i^{th} bond length, respectively, and b is a constant of 0.37 Å [38, 40]. For Fe^{2+}–O^{2-} and Fe^{3+}–O^{2-}, R_0 are 1.734 and 1.759 Å, respectively [40]. Unfortunately, the BVS method overestimates (underestimates) ionic valence as compressive (tensile) strain is applied. However, the relative valence can still distinguish Fe^{2+} and Fe^{3+} ions. Figure 4(a) shows the dependence of charge separation on lattice strain at $\lambda = 100\%$. The charge separation increases when the strain changes from -6% to 4%, but it decreases at $S > 4\%$. The change of charge separation at $S > 4\%$ is consistent with our previous results [41], which can be attributed to the fluctuation of FeB42–O bonds. The dependence of the x and z components of $\boldsymbol{R}$ on strain was also investigated. In Fig. 4(a), the increase of x and z components with strain manifests the increase and decrease of electric moment from FeB42 and FeB43, respectively. Hence, in Fig. 4(b), the resultant FE polarization decreases when the strain changes from -6% to 6%. Although the z component of $\boldsymbol{R}$ shows a decrease at $S = 6\%$, the reduced charge separation restrains the increase of FE polarization.

Based on the modern theory of polarization, the FE polarization calculated through the Berry phase for a solid is a superposition of lattices [42]. Along each crystal axis, there is a polarization quantum $PQ = eR/\Omega$, where e, R, and Ω are the elementary charge, lattice constant along a specific crystal axis, and the volume of the unit cell, respectively. The polarization quantum is a characteristic value for a specific system and it is related to the unit cell. For a long-range ordered system, the polarization can be summed with many multiple polarization quanta through calculations. Therefore, the output results from VASP should be divided by the polarization quantum. The remainder is the original state of ferroelectrics. However, the original state cannot be detected

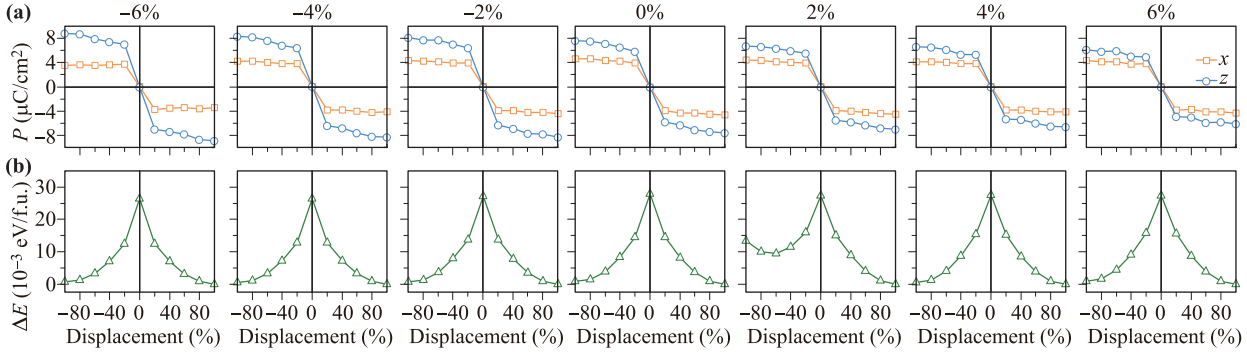

Fig. 3 Dependence of **(a)** FE polarization along the x and z axes and **(b)** total energy on ionic displacement at $-6\% \leq S \leq 6\%$.

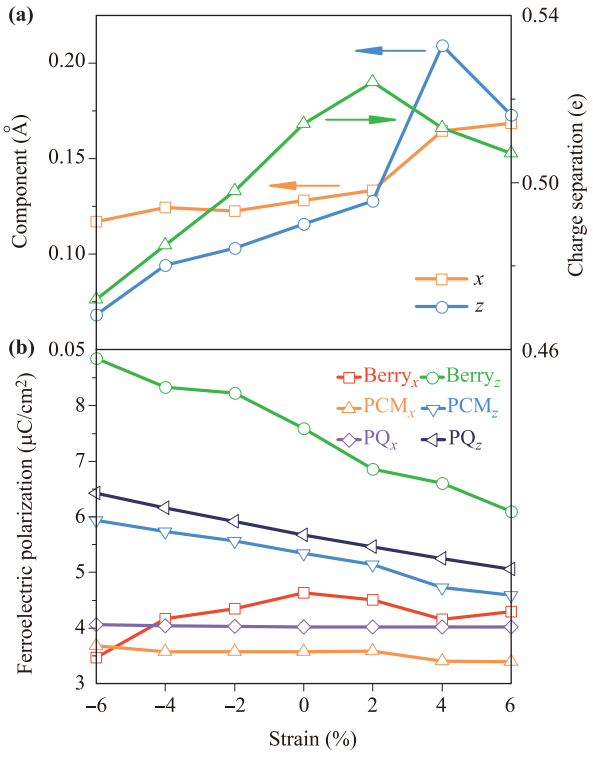

Fig. 4 **(a)** Dependence of charge separation and the x and z components of $\boldsymbol{R}$ of the FeB42–FeB43 pair on strain. **(b)** Spontaneous FE polarization along the x and z axes calculated with the Berry phase, the PCM, and the polarization quantum at $-6\% \leq S \leq 6\%$. $\lambda = 100\%$ is used for both (a) and (b).

through measurements. In experiments, the spontaneous FE polarization is usually defined by the half value of the FE polarization difference between the positive and negative biases. Actually, the difference of FE polarization is consistent with the polarization quantum. From this point of view, the spontaneous FE polarization is calculated based on the polarization quantum. Figure 4(b) shows the strain-dependent FE polarization calculated with the Berry phase, the PCM, and the half polarization quantum. The polarization quantum expression shows that the spontaneous FE polarization is directly correlated with the size of the unit cell. The polarization quantum along the x and z axes exhibits a linear-like correlation with strain. The spontaneous FE polarization estimated by using the PCM shows a correspondent trend. However, the Berry phase results show a difference from the polarization quantum and PCM results. In fact, the electrons around ions show an off-center distribution because of the Fe–O bonding, which cannot be simply evaluated by using the PCM. Similarly, the polarization quantum does not take Fe–O bonding into consideration. In Berry phase calculations, the origin of FE polarization is divided into ionic and electronic parts by using Wannier functions, which are localized in space and have been used to visualize the chemical bonding and to calculate the electronic structure [42]. The off-center electronic distribution results in extra FE polarization. The discrepancy between the Berry phase and other results indicates that the electronic distribution in monoclinic Fe_3O_4 has a large influence on FE polarization. Remarkably, as the strain changes from 6% to −6%, the FE polarization along the z axis in low-temperature monoclinic Fe_3O_4 can increase by 45.3%.

4 Conclusion

In summary, spontaneous FE polarization and strain effects on ferroelectricity of low-temperature monoclinic Fe_3O_4 are investigated. It is found that FE polarization in Fe_3O_4 originates from the noncentrosymmetric charge distribution at the FeB42–FeB43 pair. The initial direction of FE polarization as found from PCM calculations is in the $-x$ and $-z$ directions. By importing the biaxial strain along the x and y axes, FE polarization in both x and z directions can be tailored. It is found that both the ionic displacement and charge separation at the FeB42–FeB43 pair, which further influence FE polarization in low-temperature monoclinic Fe_3O_4, are affected by strain. When the strain changes from 6% to −6%, FE polarization along the z axis exhibits an increase of 45.3%.

Acknowledgements This work was supported by the National Natural Science Foundation of China (Grant Nos. 51671142 and U1632152) and the Key Project of the Natural Science Foundation of Tianjin City (Grant No. 16JCZDJC37300).

References

1. J. F. Scott, Data storage: Multiferroic memories, *Nat. Mater.* 6(4), 256 (2007)
2. N. Balke, S. Choudhury, S. Jesse, M. Huijben, Y. H. Chu, A. P. Baddorf, L. Q. Chen, R. Ramesh, and S. V. Kalinin, Deterministic control of ferroelastic switching in multiferroic materials, *Nat. Nanotechnol.* 4(12), 868 (2009)
3. M. Liu, Z. Y. Zhou, T. X. Nan, B. M. Howe, G. J. Brown, and N. X. Sun, Voltage tuning of ferromagnetic resonance with bistable magnetization switching in energy-efficient magnetoelectric composites, *Adv. Mater.* 25(10), 1435 (2013)
4. P. W. M. Blom, R. M. Wolf, J. F. M. Cillessen, and M. P. C. M. Krijn, Ferroelectric Schottky diode, *Phys. Rev. Lett.* 73(15), 2107 (1994)
5. M. Gajek, M. Bibes, S. Fusil, K. Bouzehouane, J. Fontcuberta, A. Barthélémy, and A. Fert, Tunnel junc-

tions with multiferroic barriers, *Nat. Mater.* 6(4), 296 (2007)

6. H. Kohlstedt, A. Petraru, K. Szot, A. Rüdiger, P. Meuffels, H. Haselier, R. Waser, and V. Nagarajan, Method to distinguish ferroelectric from nonferroelectric origin in case of resistive switching in ferroelectric capacitors, *Appl. Phys. Lett.* 92(6), 062907 (2008)
7. C. H. Yang, J. Seidel, S. Y. Kim, P. B. Rossen, P. Yu, M. Gajek, Y. H. Chu, L. W. Martin, M. B. Holcomb, Q. He, P. Maksymovych, N. Balke, S. V. Kalinin, A. P. Baddorf, S. R. Basu, M. L. Scullin, and R. Ramesh, Electric modulation of conduction in multiferroic Ca-doped $BiFeO_3$ films, *Nat. Mater.* 8(6), 485 (2009)
8. W. D. Wu, J. R. Guest, Y. Horibe, S. Park, T. Choi, S. W. Cheong, and M. Bode, Polarization-modulated rectification at ferroelectric surfaces, *Phys. Rev. Lett.* 104(21), 217601 (2010)
9. Ch. Binek, A. Hochstrat, X. Chen, P. Borisov, W. Kleemann, and B. Doudin, Electrically controlled exchange bias for spintronic applications, *J. Appl. Phys.* 97, 10C514 (2005)
10. Z. Zhou, X. Y. Zhang, T. F. Xie, T. X. Nan, Y. Gao, X. Yang, X. J. Wang, X. Y. He, P. S. Qiu, N. X. Sun, and D. Z. Sun, Strong non-volatile voltage control of magnetism in magnetic/antiferroelectric magnetoelectric heterostructures, *Appl. Phys. Lett.* 104(1), 012905 (2014)
11. Z. Q. Hu, T. X. Nan, X. J. Wang, M. Staruch, Y. Gao, P. Finkel, and N. X. Sun, Voltage control of magnetism in FeGaB/PIN-PMN-PT multiferroic heterostructures for high-power and high-temperature applications, *Appl. Phys. Lett.* 106(2), 022901 (2015)
12. S. Cherepov, P. Khalili Amiri, J. G. Alzate, K. Wong, M. Lewis, P. Upadhyaya, J. Nath, M. Bao, A. Bur, T. Wu, G. P. Carman, A. Khitun, and K. L. Wang, Electric-field-induced spin wave generation using multiferroic magnetoelectric cells, *Appl. Phys. Lett.* 104(8), 082403 (2014)
13. P. A. Miles, W. B. Westphal, and A. Von Hippel, Dielectric spectroscopy of ferromagnetic semiconductors, *Rev. Mod. Phys.* 29(3), 279 (1957)
14. A. Yanase and K. Siratori, Band structure in the high temperature phase of Fe_3O_4, *J. Phys. Soc. Jpn.* 53(1), 312 (1984)
15. J. P. Attfield, The Verwey phase of magnetite: A long-running mystery in ferrites, *J.Jpn. Soc. Powder Powder Metall.* 61(S1), S43 (2014)
16. E. J. Verwey, Electronic conduction of magnetite (Fe_3O_4) and its transition point at low temperatures, *Nature* 144(3642), 327 (1939)
17. M. Alexe, M. Ziese, D. Hesse, P. Esquinazi, K. Yamauchi, T. Fukushima, S. Picozzi, and U. Gösele, Ferroelectric switching in multiferroic magnetite (Fe_3O_4) thin films, *Adv. Mater.* 21(44), 4452 (2009)
18. K. Kato and S. Iida, Magnetoelectric effects of Fe_3O_4 at 4.2 K, *J. Phys. Soc. Jpn.* 50(9), 2844 (1981)
19. K. Yamauchi, T. Fukushima, and S. Picozzi, Ferroelectricity in multiferroic magnetite Fe_3O_4 driven by noncentrosymmetric Fe^{2+}/Fe^{3+} charge-ordering: First-principles study, *Phys. Rev. B* 79(21), 212404 (2009)
20. K. Kato and S. Iida, Observation of ferroelectric hysteresis loop of Fe_3O_4 at 4.2 K, *J. Phys. Soc. Jpn.* 51(5), 1335 (1982)
21. Y. Miyamoto and K. Ishiyama, Measurement of spontaneous electric polarization in magnetite (Fe_3O_4) at 4.2 K, *Solid State Commun.* 87(6), 581 (1993)
22. R. D. King-Smith and D. Vanderbilt, Theory of polarization of crystalline solids, *Phys. Rev. B* 47(3), 1651 (1993)
23. D. Vanderbilt and R. D. King-Smith, Electric polarization as a bulk quantity and its relation to surface charge, *Phys. Rev. B* 58(7), 4442 (1993)
24. R. Resta, Macroscopic polarization in crystalline dielectrics: The geometric phase approach, *Rev. Mod. Phys.* 66(3), 899 (1994)
25. J. B. Neaton, C. Ederer, U. V. Waghmare, N. A. Spaldin, and K. M. Rabe, First-principles study of spontaneous polarization in multiferroic $BiFeO_3$, *Phys. Rev. B* 71(1), 014113 (2005)
26. G. Kresse and J. Furthmüller, Efficient iterative schemes for ab initio total-energy calculations using a plane-wave basis set, *Phys. Rev. B* 54(16), 11169 (1996)
27. P. E. Blöchl, Projector augmented-wave method, *Phys. Rev. B* 50(24), 17953 (1994)
28. H. T. Jeng, G. Y. Guo, and D. J. Huang, Charge-orbital ordering in low-temperature structures of magnetite: GGA+U investigations, *Phys. Rev. B* 74(19), 195115 (2006)
29. J. P. Perdew and Y. Wang, Accurate and simple analytic representation of the electron-gas correlation energy, *Phys. Rev. B* 45(23), 13244 (1992)
30. V. I. Anisimov, J. Zaanen, and O. K. Andersen, Band theory and Mott insulators: Hubbard U instead of Stoner I, *Phys. Rev. B* 44(3), 943 (1991)
31. A. I. Liechtenstein, V. I. Anisimov, and J. Zaanen, Density-functional theory and strong interactions: Orbital ordering in Mott–Hubbard insulators, *Phys. Rev. B* 52(8), R5467 (1995)
32. M. S. Senn, J. P. Wright, and J. P. Attfield, Charge order and three-site distortions in the Verwey structure of magnetite, *Nature* 481(7380), 173 (2011)
33. M. I. Aroyo, J. M. Perez-Mato, C. Capillas, E. Kroumova, S. Ivantchev, G. Madariaga, A. Kirov, and H. Wondratschke, Bilbao crystallographic server (I): Databases and crystallographic computing programs, *Zeitschrift für Kristallographie-Cryst. Mater.* 221, 15 (2006)
34. M. I. Aroyo, A. Kirov, C. Capillas, J. M. Perez-Mato, and H. Wondratschek, Bilbao Crystallographic Server II: Representations of crystallographic point groups and space groups, *Acta Crystallogr. A* 62(2), 115 (2006)

35. M. I. Aroyo, J. M. Perez-Mato, D. Orobengoa, E. Tasci, G. de la Flor, and A. Kirov, Crystallography online: Bilbao crystallographic server, *Izv. Him.* 43, 183 (2011)

36. P. Baettig, C. Ederer, and N. A. Spaldin, First principles study of the multiferroics $BiFeO_3$, Bi_2FeCrO_6, and $BiCrO_3$: Structure, polarization, and magnetic ordering temperature, *Phys. Rev. B* 72(21), 214105 (2005)

37. X. Y. Hou, X. C. Wang, G. F. Chen, and W. B. Mi, Electric field tunable half-metallic characteristic at $Fe_3O_4/BaTiO_3$ interfaces, *Phys. Chem. Chem. Phys.* 19(6), 4330 (2017)

38. I. D. Brown and D. Altermatt, Bond-valence parameters obtained from a systematic analysis of the inorganic crystal structure database, *Acta Crystallogr. B* 41(4), 244 (1985)

39. I. D. Brown, Chemical and steric constrains in inorganic solids, *Acta Cyrst. B* 48(5), 553 (1992)

40. N. E. Brese and M. O'Keeffe, Bond-valence parameters for solids, *Acta Crystallogr. B* 47(2), 192 (1991)

41. X. Liu, L. Yin, and W. B. Mi, Biaxial strain effect induced electronic structure alternation and trimeron recombination in Fe_3O_4, *Sci. Rep.* 7, 43403 (2017)

42. N. A. Spaldin, A beginner's guide to the modern theory of polarization, *J. Solid State Chem.* 195, 2 (2012)